NACA

RESEARCH MEMORANDUM

A FREE-FLIGHT TECHNIQUE FOR MEASURING DAMPING IN ROLL BY USE OF ROCKET-POWERED MODELS AND SOME INITIAL RESULTS FOR RECTANGULAR WINGS

By James L. Edmondson and E. Claude Sanders, Jr.

Langley Aeronautical Laboratory
Langley Air Force Base, Va.

NATIONAL ADVISORY COMMITTEE
FOR AERONAUTICS

WASHINGTON
December 20, 1949

NATIONAL ADVISORY COMMITTEE FOR AERONAUTICS

RESEARCH MEMORANDUM

A FREE-FLIGHT TECHNIQUE FOR MEASURING DAMPING IN ROLL BY USE OF ROCKET-POWERED MODELS AND SOME INITIAL RESULTS FOR RECTANGULAR WINGS

By James L. Edmondson and E. Claude Sanders, Jr.

SUMMARY

A simplified method for obtaining free-flight measurements of damping in roll through use of rocket-powered models has been developed; and initial configurations have been tested through a Mach number range of approximately 0.85 to 1.40, which corresponds to a Reynolds number range of 4.5×10^6 to 8×10^6. The basic principle of this method is that the model is forced to roll by a nonaerodynamic rolling moment of known magnitude which is produced by a canted-nozzle assembly, and the damping in roll is computed by balancing the moments acting on the model.

The initial configurations tested and reported herein had rectangular wings of aspect ratio 3.71 and NACA 65A009 and NACA 65A006 airfoil sections. The damping in roll is maintained through transonic speeds and is somewhat less than wing theory at supersonic speeds.

INTRODUCTION

A simplified method for obtaining damping in roll experimentally at transonic and supersonic speeds has been developed which utilizes a simple rocket-powered model adaptable to systematic testing. A known nonaerodynamic forcing moment produces roll; and, by measurements of the inertia of the model, Mach number, and rolling velocity, the damping in roll can be determined with reasonable accuracy. A description of the method and results of the initial flight tests are reported herein.

The two initial configurations tested were 1.3-scale models of roll-control-effectiveness configurations 50 and 51 of reference 1 with rectangular wings of aspect ratio 3.71 and NACA 65A006 and NACA 65A009 airfoil sections. The damping-in-roll coefficient was

obtained for these configurations from a Mach number range of approximately 0.85 to 1.40, corresponding to an approximate Reynolds number range of 4.5×10^6 to 8×10^6. These flight tests were conducted at the Pilotless Aircraft Research Test Station, Wallops Island, Va.

SYMBOLS

C_l rolling-moment coefficient $\left(\frac{L}{qSb}\right)$

C_{l_p} damping-in-roll coefficient $\left(\frac{\partial C_l}{\partial \frac{pb}{2V}}\right)$

$C_{l_{\delta_a}}$ rolling-moment-effectiveness coefficient $\left(\frac{\partial C_l}{\partial \delta_a}\right)$

δ_a angular deflection of one aileron, degrees (equally deflected ailerons on all wing panels)

C_{l_o} out-of-trim rolling-moment coefficient $\left(\frac{L_o}{qSb}\right)$

C_D total-drag coefficient $\left(\frac{D}{qS}\right)$

D total drag, pounds

L rolling moment, foot-pounds

L_p rate of change of rolling moment with rolling velocity, $\frac{\text{foot-pounds}}{\text{radians per second}}$

L_o out-of-trim rolling moment, foot-pounds

F thrust, pounds

T torque, pound-foot

$\dot{\varphi}$, p rolling angular velocity, radians per second

$\ddot{\varphi}$ rolling angular acceleration, radians per second^2

V forward velocity, feet per second

[redacted]

a	longitudinal acceleration, feet per second^2
g	acceleration due to gravity, feet per second^2
$\frac{pb}{2V}$	helix angle generated by wing tip in roll, radians
q	dynamic pressure, pounds per square foot
M	Mach number
A	aspect ratio $\left(\frac{b^2}{S'}\right)$
b	wing span, feet (diameter of circle generated by wing tips)
S'	total wing area of two wings, square feet (wing panel assumed to extend to model center line)
S	total wing area of three wings, square feet (wing panel assumed to extend to model center line)
d	distance from center line of model to center line of individual units of nozzle assembly, inches
W	weight, pounds
I_x	moment of inertia about longitudinal axis, slug-feet^2
M_θ	wing-torsional-stiffness parameter, inch-pound per degree (twisted and measured at wing tip)
γ	angle of flight path to horizontal, degrees

Subscripts:

1	sustainer-on flight
2	coasting flight

MODEL AND APPARATUS

Model

A sketch of the models used in this investigation is shown in figure 1. The models are simply constructed with minimum internal instrumentation to allow systematic flight testing of various wing configurations. A complete model, as shown in figure 2, consists of a wooden fuselage with reinforced wooden wings, a nose containing batteries and spinsonde, a ballast tube that attaches to rocket-motor head cap, and a rocket motor with canted nozzles. The installation of the rocket motor with canted nozzles is shown in figure 3. The canted-nozzle assembly consists of four small nozzles which are offset from the center line of the model and set at an angle to provide the desired torque.

Apparatus

The apparatus used to obtain the required data were:

(a) A spinsonde in the nose of the model which transmits a polarized signal

(b) A spinsonde receiver on the ground which receives the polarized signal and records a time history of rolling velocity

(c) A continuous-wave Doppler radar unit which records a time history of forward velocity

(d) Radiosonde equipment which records atmospheric data at the time of the flight

The forward velocity from the Doppler radar record is combined with static pressure and speed of sound from the radiosonde record to compute dynamic pressure and Mach number, respectively.

The models are boosted from a rail-type launching stand, as shown in figure 4.

TECHNIQUE

The basic principle of this technique is that the model is forced to roll by a nonaerodynamic rolling moment of known magnitude which is produced by the canted-nozzle assembly, and the damping in roll is computed by balancing the moments acting on the model. The moments

[redacted]

causing roll are produced by the torque of the canted nozzle and the out of trim due to unavoidable misalinement of component parts of the model. The moments opposing roll are produced by the inertia of the model and damping in roll of the wings and body. For one degree of freedom, the equation for equilibrium can be written

$$I_x\ddot{\varphi} - L_p\dot{\varphi} = T + L_o \tag{1}$$

or in coefficient form

$$I_x\ddot{\varphi} - C_{l_p}\frac{b}{2V}qSb\dot{\varphi} = T + C_{l_o}qSb \tag{2}$$

Because both damping moment and out-of-trim moment are unknown, two conditions must be found for the same Mach number. This is accomplished by using both sustainer-on flight (denoted by subscript 1) and coasting flight (denoted by subscript 2). Now the equations are

$$\frac{I_{x_1}\ddot{\varphi}_1}{q_1Sb} - C_{l_p}\frac{b}{2V_1}\dot{\varphi}_1 = \frac{T}{q_1Sb} + C_{l_o} \tag{3}$$

$$\frac{I_{x_2}\ddot{\varphi}_2}{q_2Sb} - C_{l_p}\frac{b}{2V_2}\dot{\varphi}_2 = C_{l_o} \tag{4}$$

Solving these two equations, assuming C_{l_o} is the same for conditions 1 and 2, yields

$$-C_{l_p} = \frac{\frac{T}{q_1} - \left(\frac{I_{x_1}\ddot{\varphi}_1}{q_1} - \frac{I_{x_2}\ddot{\varphi}_2}{q_2}\right)}{\frac{Sb^2}{2}\left(\frac{\dot{\varphi}_1}{V_1} - \frac{\dot{\varphi}_2}{V_2}\right)} \tag{5}$$

The rolling acceleration term of equation (5) is a small factor in the evaluation of C_{l_p} in this case, but is easily applied by a faired point-by-point differentiation of the rolling-velocity-versus-time curve and by measuring the inertia characteristics of the model. The inertia of the model is measured with the rocket motor loaded (launching condition) and empty (burnout condition). The inertia is constant during decelerating flight (burnout condition); however, it is necessary to compute the inertia during the accelerating flight while the powder

grain is burning. The grain is assumed to burn so that the radius of gyration of the grain remains constant; therefore, the inertia of the grain varies as the mass. Since the mass is burned at a constant rate, the inertia will be linear with burning time - the two end points being known.

The torque produced by the canted nozzle can be determined in two ways. The total impulse of all rocket motors of the type used in this investigation is constant so that the thrust of each motor can be determined by comparison with ground tests knowing the ratio of burning times. The torque produced by the canted nozzle is then computed by the relation

$$T = Fd \tan(\text{cant angle}) \tag{6}$$

The other method which can be used involves computing the torque from the rocket thrust obtained from flight measurements of accelerations during sustainer-on and coasting portions of the flight. The thrust is computed from the flight data by the relationship between accelerations at the same Mach number.

$$\frac{a_1}{g} = \frac{F - D_1}{W_1} - \sin \gamma_1$$

$$\frac{a_2}{g} = \frac{-D_2}{W_2} - \sin \gamma_2$$

Solving these two equations assuming $C_{D_1} = C_{D_2}$ yields

$$F = W_1\left(\frac{a_1}{g} + \sin \gamma_1\right) - \frac{q_1}{q_2} W_2\left(\frac{a_2}{g} + \sin \gamma_2\right) \tag{7}$$

This equation does not consider a correction for base drag because this correction appeared to be small in the present case. The torques computed from flight data were corrected to the burning time of the ground tests with total impulse remaining constant. The two extreme cases are plotted against time and compared to the ground test in figure 5. All the other torque-time curves fell within these limits. Part of the difference in torque shown may be due to an error in calculating the burning times of the rocket motors used in flight. This error would affect only the comparison shown in figure 5 because the actual torques used to calculate C_{l_p} were computed by the second method outlined above, which does not depend upon burning time for accuracy.

An evaluation of the factors that can cause an error in C_{l_p} is obtained by an analysis of equation (5). The relative magnitudes of the terms in the numerator are such that the omission of the parentheses containing the $\ddot{\phi}$ terms would cause about 2-percent error in C_{l_p} at supersonic speeds and about 8-percent error at transonic speeds. The factors capable of producing their own order of magnitude of error in C_{l_p} are the terms containing torque T and rolling velocity $\dot{\phi}$. From the methods of recording and computing the torque and rolling velocity used in these calculations, the accuracy of the magnitude of C_{l_p} for any one model is estimated to be within ±10 percent of a mean value. This accuracy is increased by the use of two or more identical models.

RESULTS AND DISCUSSION

Three identical models of each configuration were flight-tested to allow evaluation of this method of testing. These models were boosted to a Mach number of approximately 0.8 before the sustainer with canted nozzles was fired; therefore, no data were obtained below this speed. Typical curves of forward velocity and rolling velocity plotted against time and tip helix angle plotted against Mach number are presented in figures 6 and 7, respectively. The effect of the torque produced by the canted nozzles on the rolling velocity can readily be seen in these figures.

Rolling velocity for the three identical configurations with NACA 65A009 airfoil section is plotted against Mach number in figure 8(a). Incomplete spinsonde data were recorded for one of these models; only the coasting portion of the flight was recorded. This portion of the curve is shown for comparison purposes even though damping in roll could not be computed for this model. The trends of these curves are consistent in that the sign of $\dot{\phi}$ reverses through transonic speeds during coasting flight; however, the magnitudes vary because of the varying degree of unavoidable out-of-trim moment, as can be seen during the coasting portion of these curves. The rolling velocity due to out-of-trim moment reverses through the transonic speed region and is less effective at supersonic speeds than at subsonic speeds. In fact, the out-of-trim moment on model 2B became ineffective at supersonic speeds. The cause of the out-of-trim moment is not known, but is believed to be largely due to misalinement of the wings (incidence).

Rolling velocity for the three identical configurations with NACA 65A006 airfoil section wings is plotted against Mach number in figure 8(b). It is interesting to note, in figure 8, the reversal of

the out-of-trim rolling velocity for the 9-percent-thick wing, indicating lateral trim instability in the transonic region, and no reversal for the 6-percent-thick wing. Evidently this reversal is a wing-thickness effect and may be overcome by utilizing very thin wing sections.

The damping-in-roll coefficient is plotted against Mach number in figure 9(a) for an NACA 65A009 airfoil section wing and in figure 9(b) for an NACA 65A006 airfoil section wing. Subsonic experimental data for a similar wing (NACA 16-009), reported in reference 2, are shown in figure 9(a), and supersonic wing theory (reference 3) is shown in both figures 9(a) and 9(b). It can be seen that the damping in roll for both airfoil sections is maintained through the transonic speed region, although a tendency toward decreased damping is shown. The supersonic values of C_{l_p} are fairly constant up to the highest Mach number of these tests.

Having determined the damping in roll for these configurations, the aileron rolling effectiveness may now be established by comparison with roll-control tests reported in reference 4. Inasmuch as the damping in roll is fairly constant in comparison with the variation of $\frac{pb/2V}{\delta_a}$ of the roll-control tests, the trend of the aileron rolling effectiveness $C_{l_{\delta_a}}$ will be similar to that of $\frac{pb/2V}{\delta_a}$ through the transonic and supersonic speed range of these tests. Therefore, the reduction in $\frac{pb/2V}{\delta_a}$ during the transonic speeds (reference 4) is caused by a reduction in aileron rolling effectiveness.

Using the values of $\frac{pb/2V}{\delta_a}$ for the NACA 65A009 section wing as presented in reference 4 and C_{l_p} for model 2A from figure 9(a), $C_{l_{\delta_a}}$ was computed by the relation

$$C_{l_{\delta_a}} = C_{l_p}\frac{pb/2V}{\delta_a}$$

where δ_a is the angular deflection of one 0.20-chord, full-span aileron; all wing panels have identical ailerons deflected equally. These values of $C_{l_{\delta_a}}$ are plotted against Mach number in figure 10.

Total-drag coefficient was obtained for these models and is plotted against Mach number in figure 11 with the total-drag coefficient for the similar roll-control-effectiveness configuration of reference 1. The total-drag coefficient for the roll-control-effectiveness models with 0.20-chord, full-span ailerons deflected approximately 5° (reference 1) was adjusted so that C_D in figure 11 is based upon total area S, extending into fuselage center lines, for direct comparison with the present results with 0° aileron deflection. The total-drag coefficients agree at subsonic speeds, but the drag of the roll-control-effectiveness model with the deflected aileron and larger tip helix angle (about 0.06 radians max.) is greater at supersonic speeds.

CONCLUDING REMARKS

The accuracy of C_{l_p} determined by this canted-nozzle technique is dependent mainly upon the accuracy to which the torque and rolling velocity can be determined. From the methods used in the present tests for determining these factors, the accuracy of the magnitude of C_{l_p} for any one model is estimated to be within ±10 percent of a mean value.

The results of these tests show that damping in roll is maintained through transonic speeds and is somewhat less than wing theory at supersonic speeds. Inasmuch as the damping-in-roll coefficient is essentially constant in comparison with $\frac{pb/2V}{\delta_a}$ (reference 4) through the transonic and supersonic speed range of these tests, the trend of the aileron-rolling-effectiveness parameter $C_{l_{\delta_a}}$ will be similar to that of $\frac{pb/2V}{\delta_a}$ from roll-control-effectiveness tests of this wing.

Langley Aeronautical Laboratory
National Advisory Committee for Aeronautics
Langley Air Force Base, Va.

REFERENCES

1. Sandahl, Carl A., and Marino, Alfred A.: Free-Flight Investigation of Control Effectiveness of Full-Span 0.2-Chord Plain Ailerons at High Subsonic, Transonic, and Supersonic Speeds to Determine Some Effects of Section Thickness and Wing Sweepback. NACA RM L7D02, 1947.

2. Johnson, Harold S.: Wind-Tunnel Investigation at Low Transonic Speeds of the Effects of Number of Wings on the Lateral-Control Effectiveness of an RM-5 Test Vehicle. NACA RM L9H16, 1949.

3. Harmon, Sidney M.: Stability Derivatives of Thin Rectangular Wings at Supersonic Speeds. Wing Diagonal ahead of Tip Mach Lines. NACA TN 1706, 1948.

4. Sandahl, Carl A., Bland, William M., Jr., and Strass, H. Kurt: Effects of Some Airfoil-Section Variations on Wing-Aileron Rolling Effectiveness and Drag as Determined in Free Flight at Transonic and Supersonic Speeds. NACA RM L9D12, 1949.

[redacted]

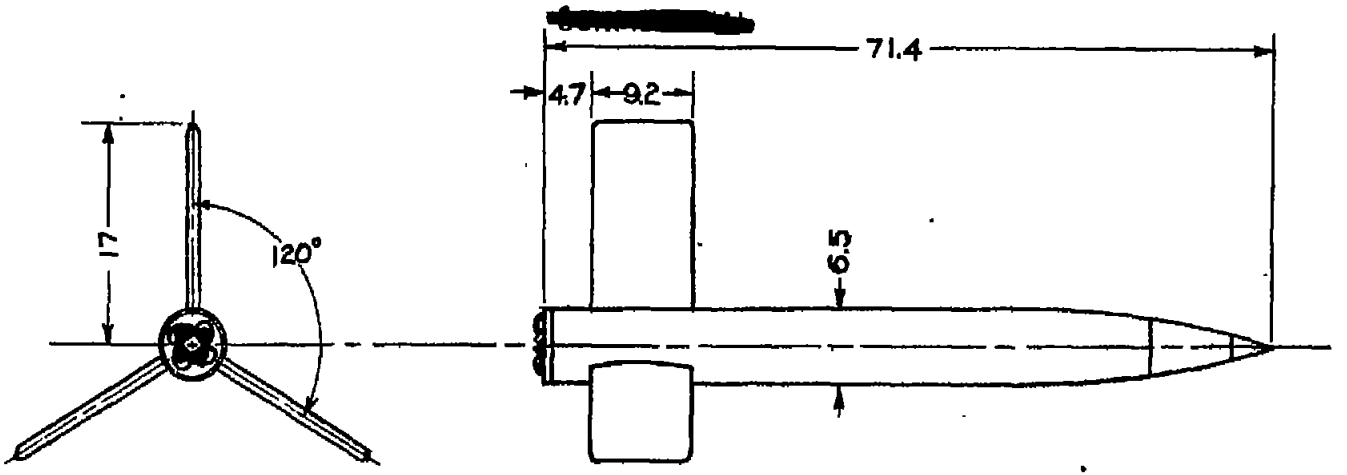

Model	Aspect Ratio	Sweep (deg)	Taper Ratio	NACA Airfoil Section	Av. M_θ at tip $\left(\frac{\text{in-lb}}{\text{deg}}\right)$	Similar RM-5 Model
1 A	3.71	0	1.0	65A006	710	51
1 B	3.71	0	1.0	65A006	750	51
1 C	3.71	0	1.0	65A006	810	51
2 A	3.71	0	1.0	65A009	1810	50
2 B	3.71	0	1.0	65A009	1740	50
2 C	3.71	0	1.0	65A009	1890	50

Figure 1.— Sketch and physical properties of initial damping-in-roll research vehicles. All dimensions in inches.

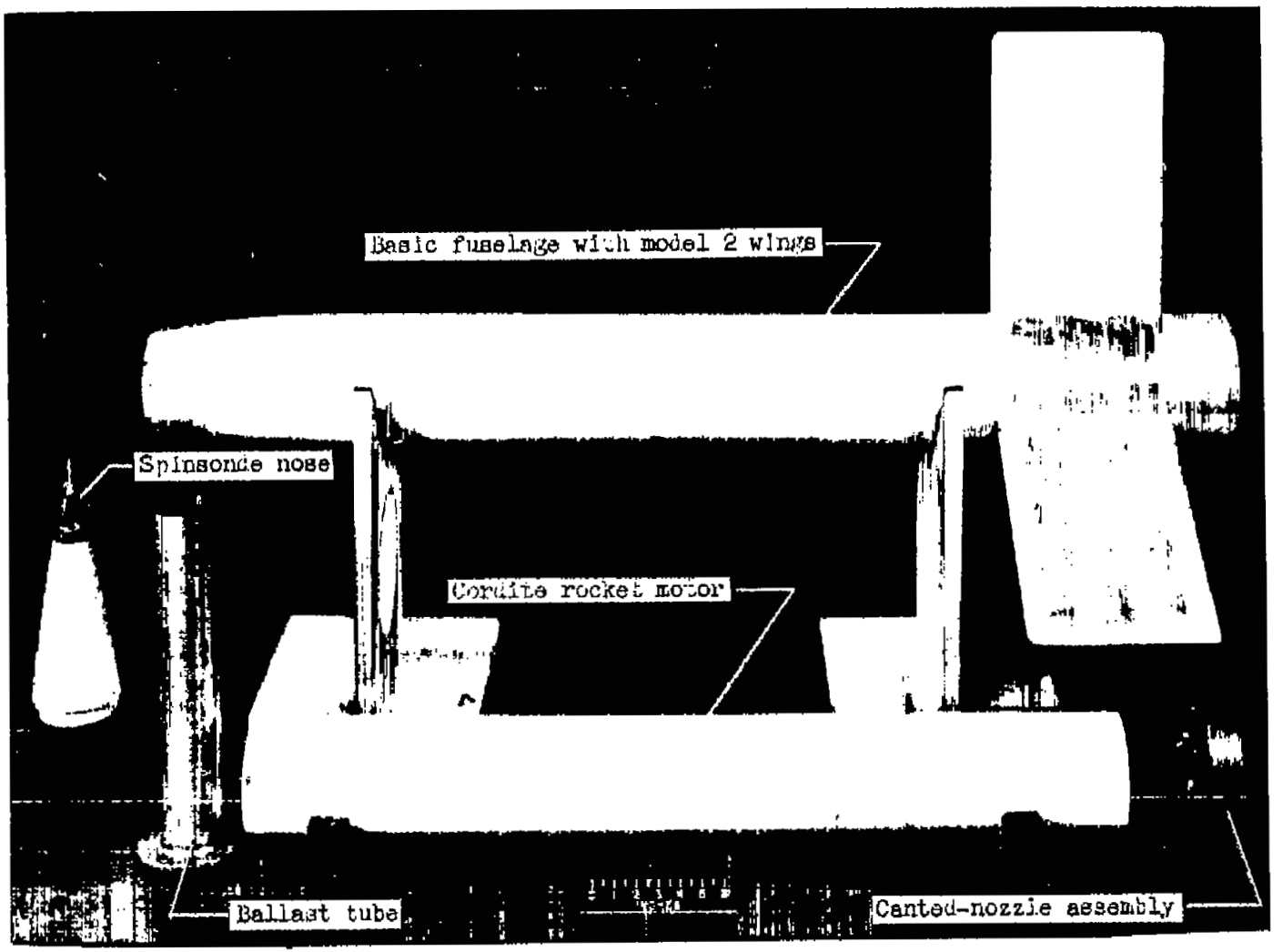

NACA

L-58815

Figure 2.- Component parts of a damping-in-roll research vehicle.

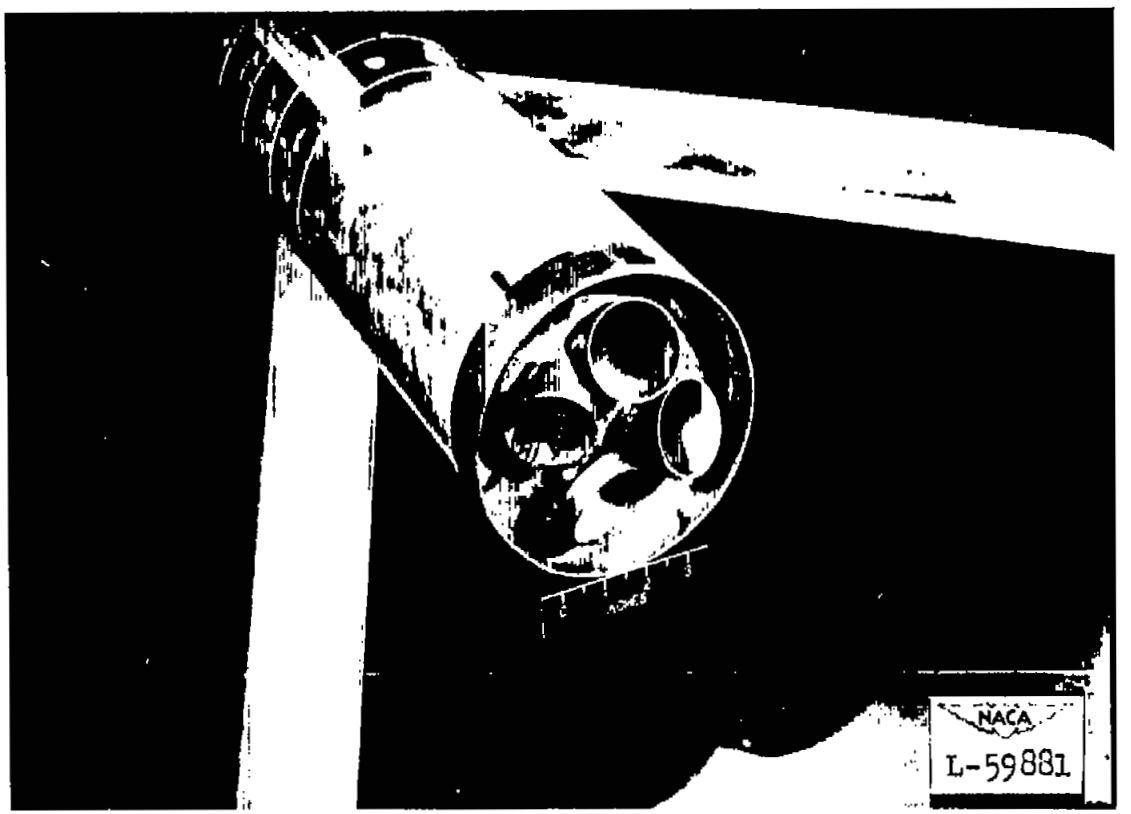

Figure 3.– Rear view of a research vehicle showing the installation of the canted-nozzle assembly.

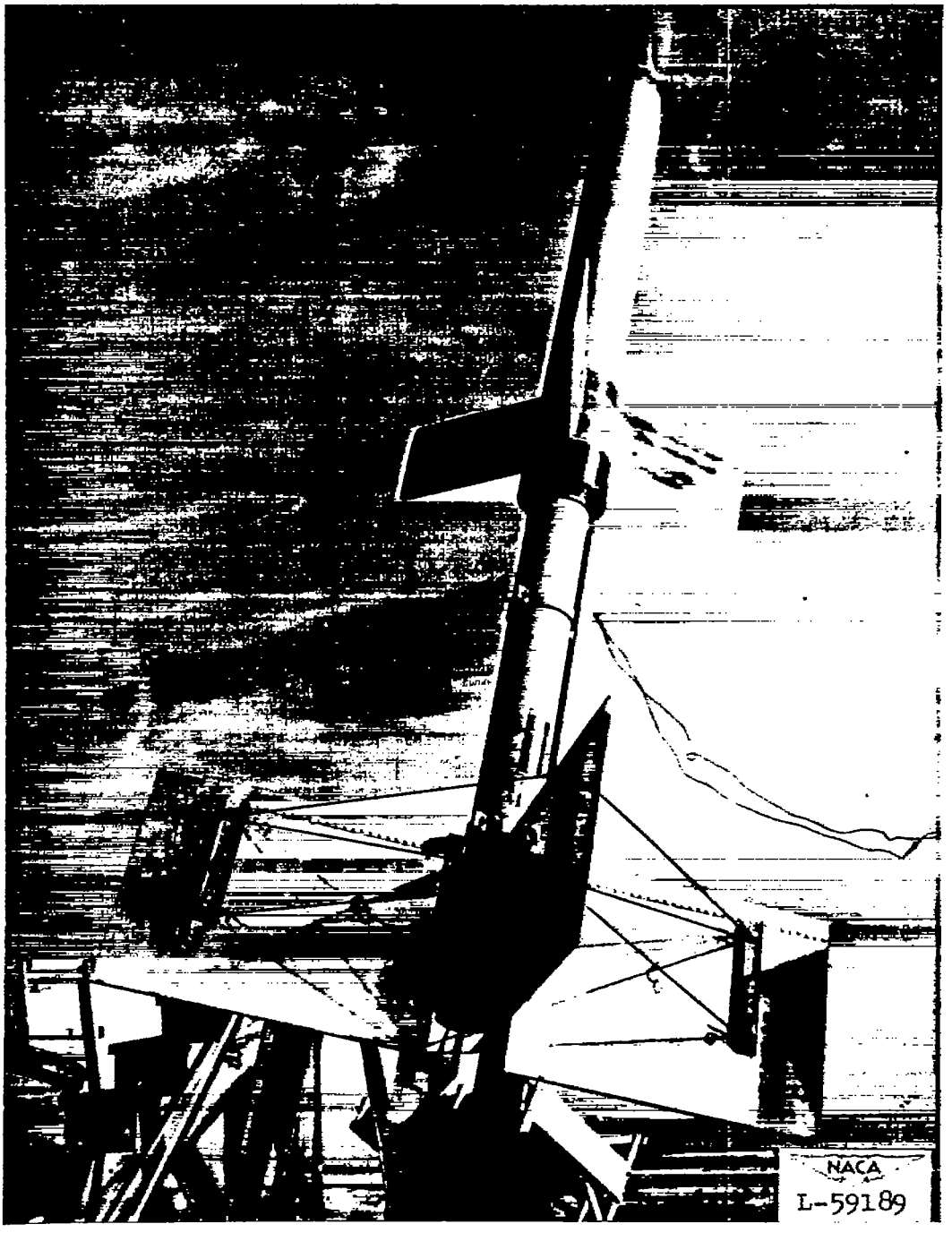

Figure 4.— Research vehicle—booster combination in firing position on a rail-type launching stand.

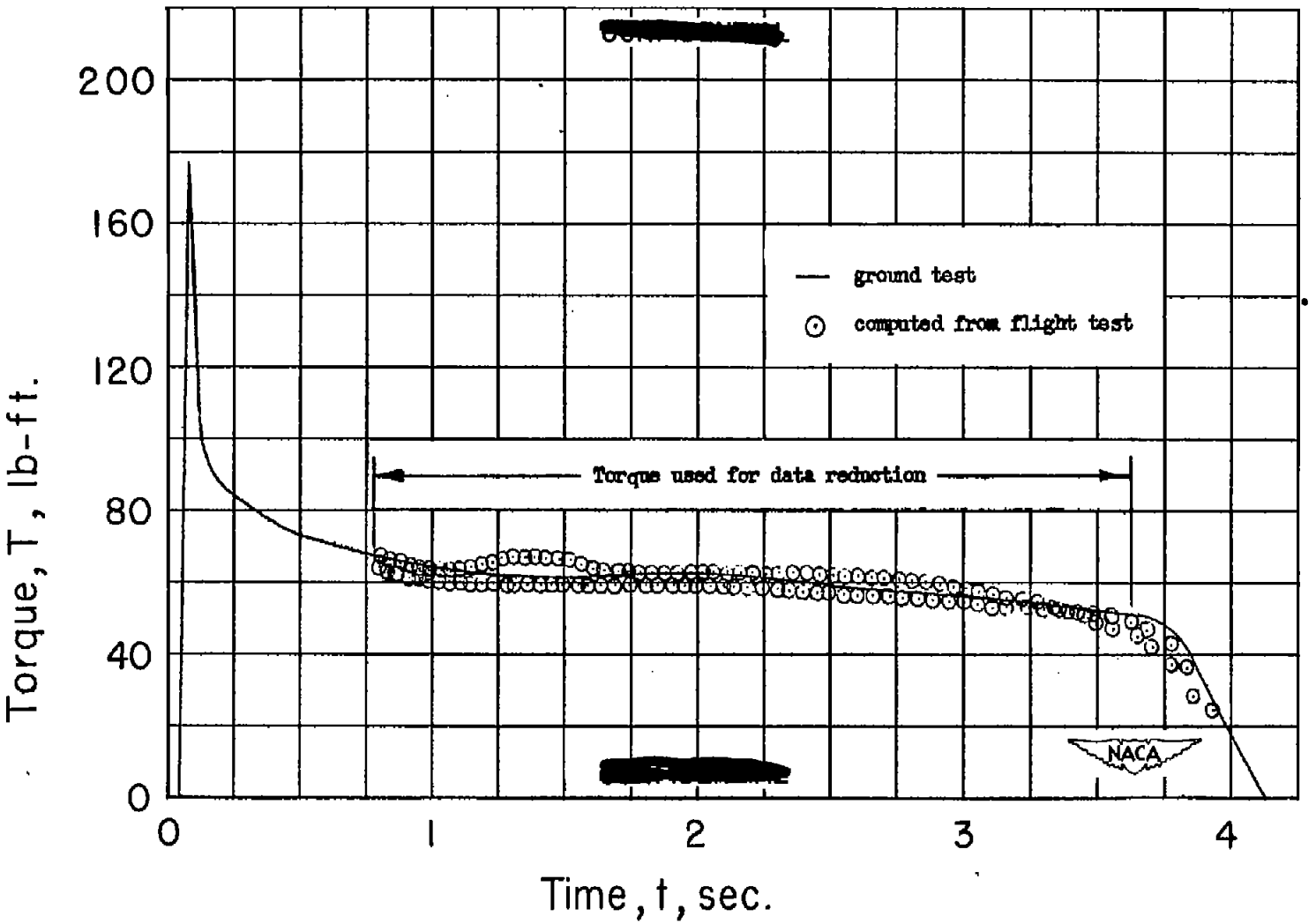

Figure 5.– Comparison of computed torque with ground test.

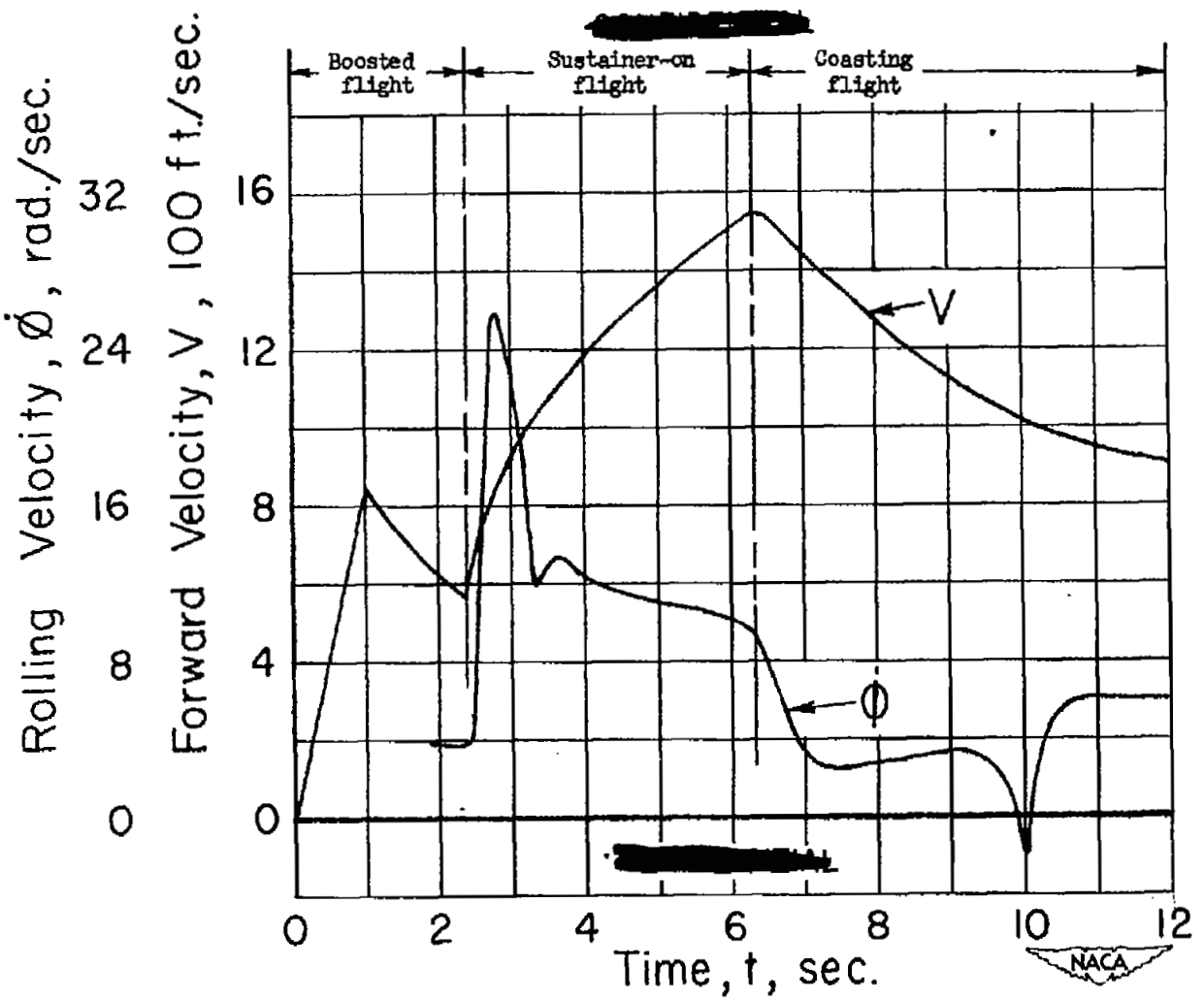

Figure 6.– Typical time history of rolling velocity and forward velocity.

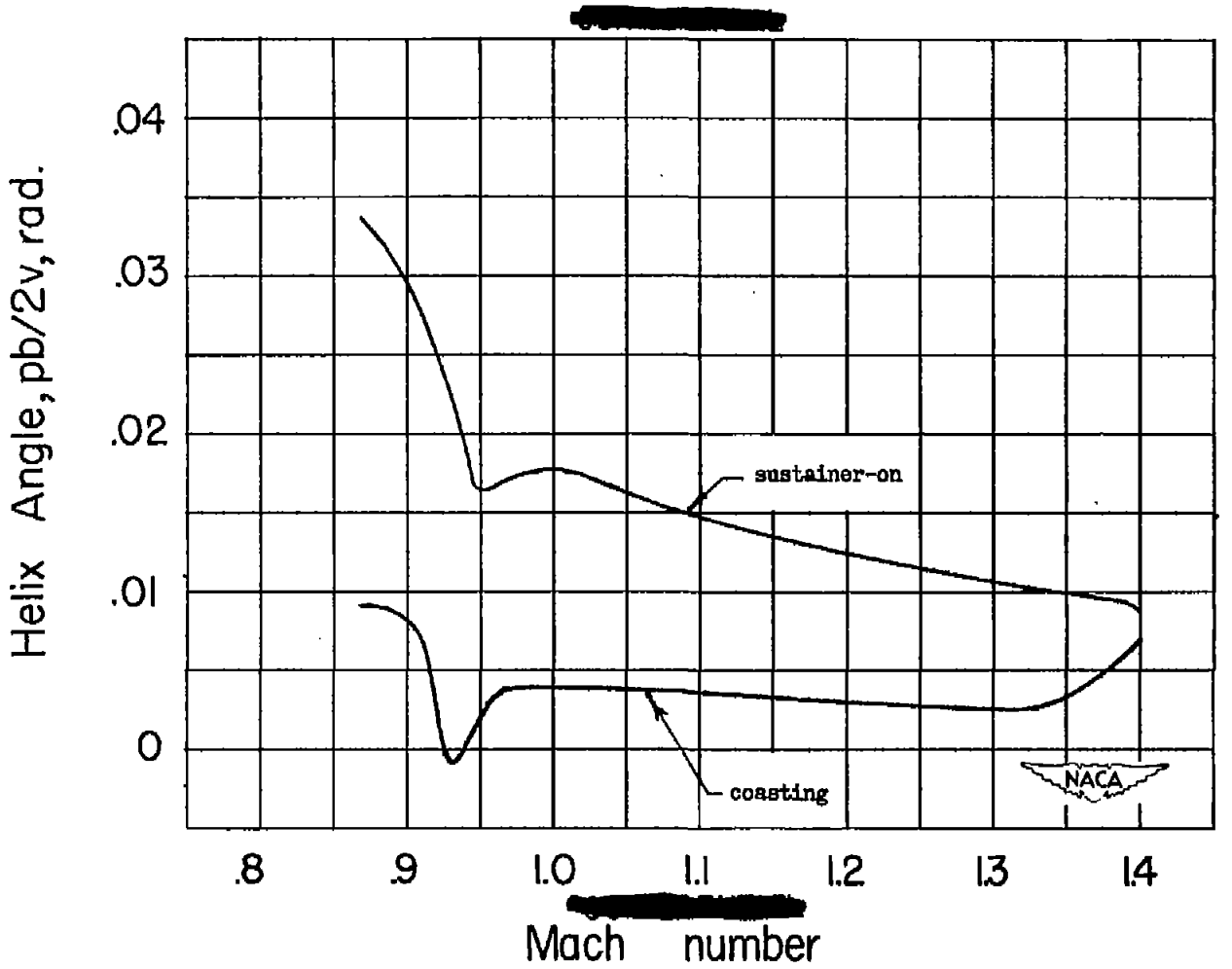

Figure 7.– Typical variation of helix angle with Mach number.

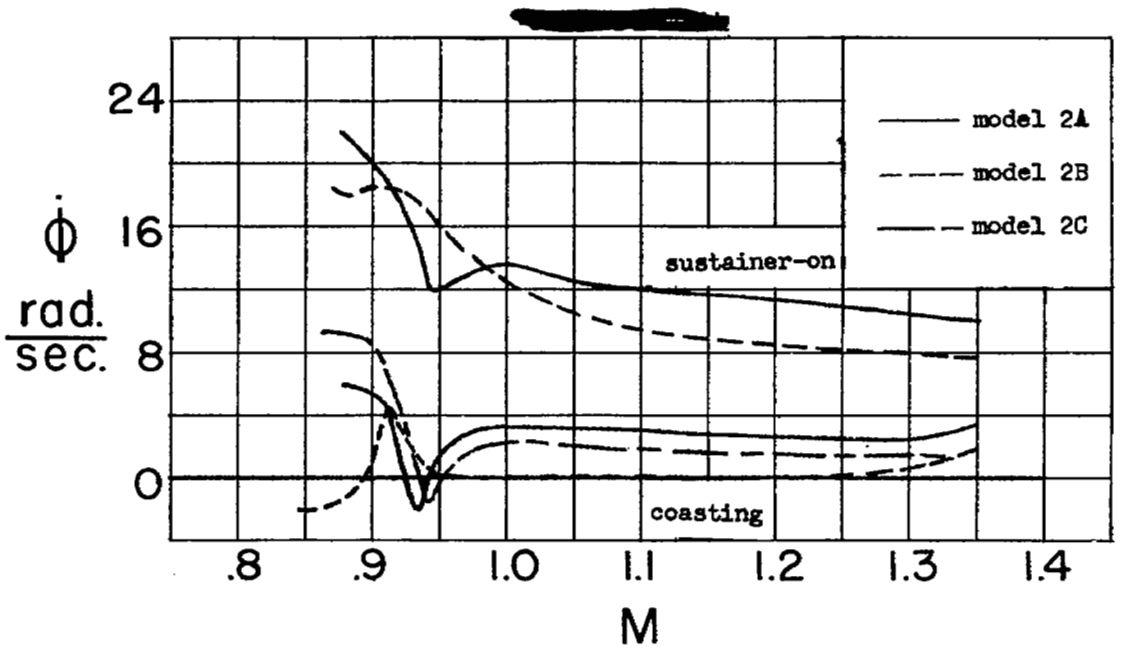

(a) NACA 65A009 airfoil section.

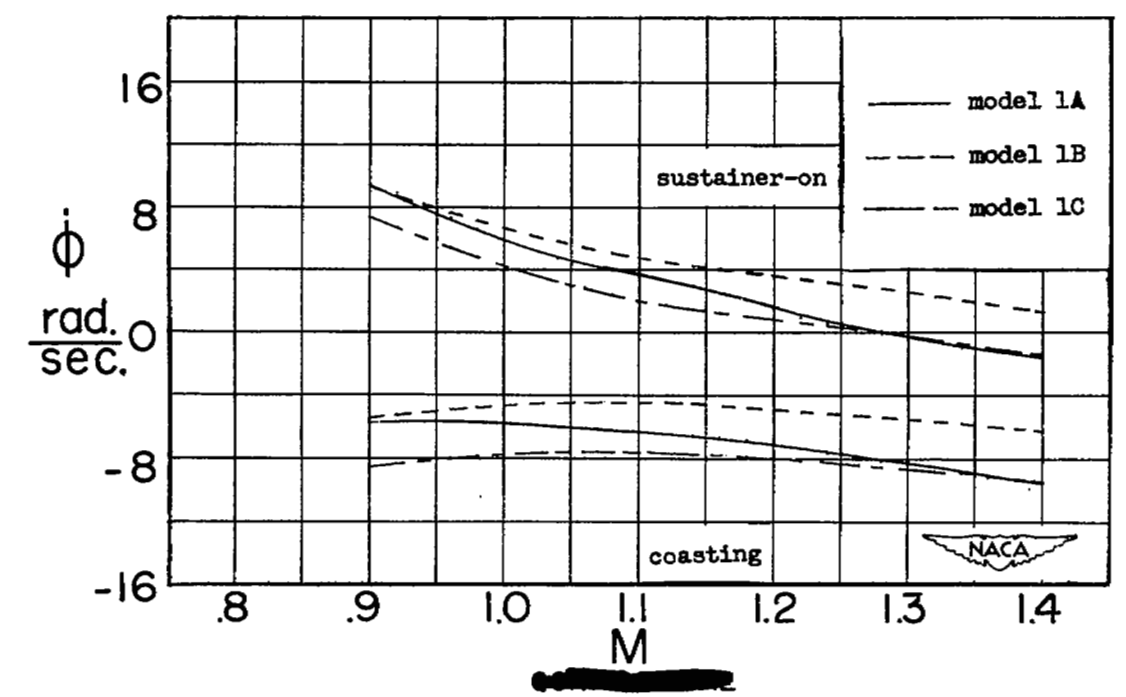

(b) NACA 65A006 airfoil section.

Figure 8.— Variation of rolling velocity with Mach number.

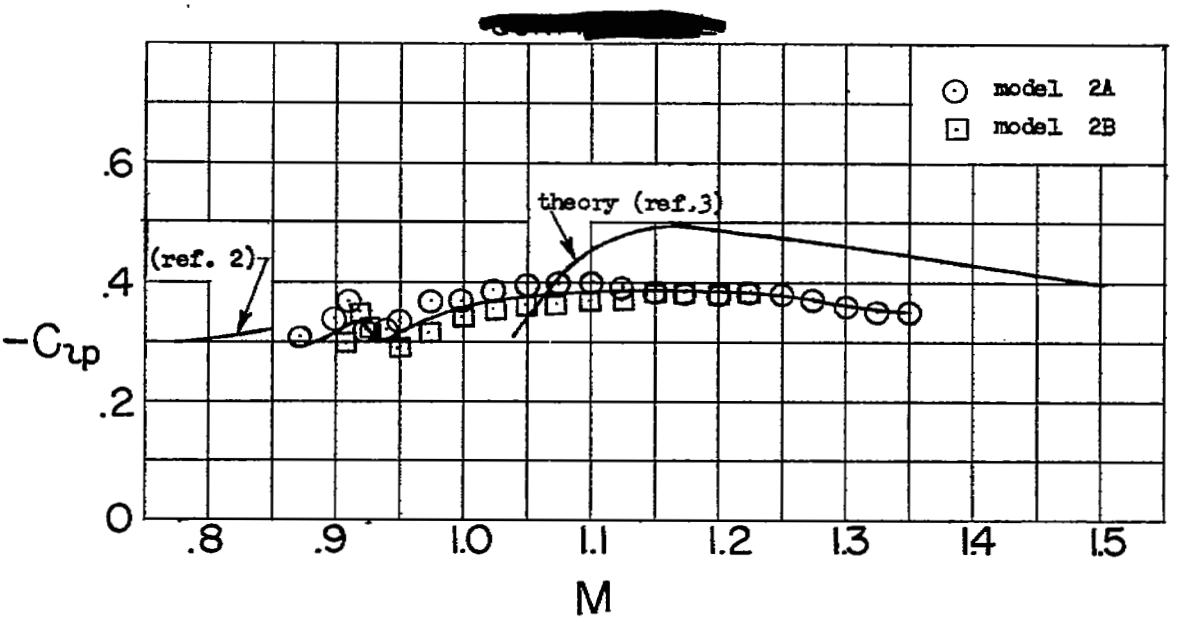

(a) NACA 65A009 airfoil section.

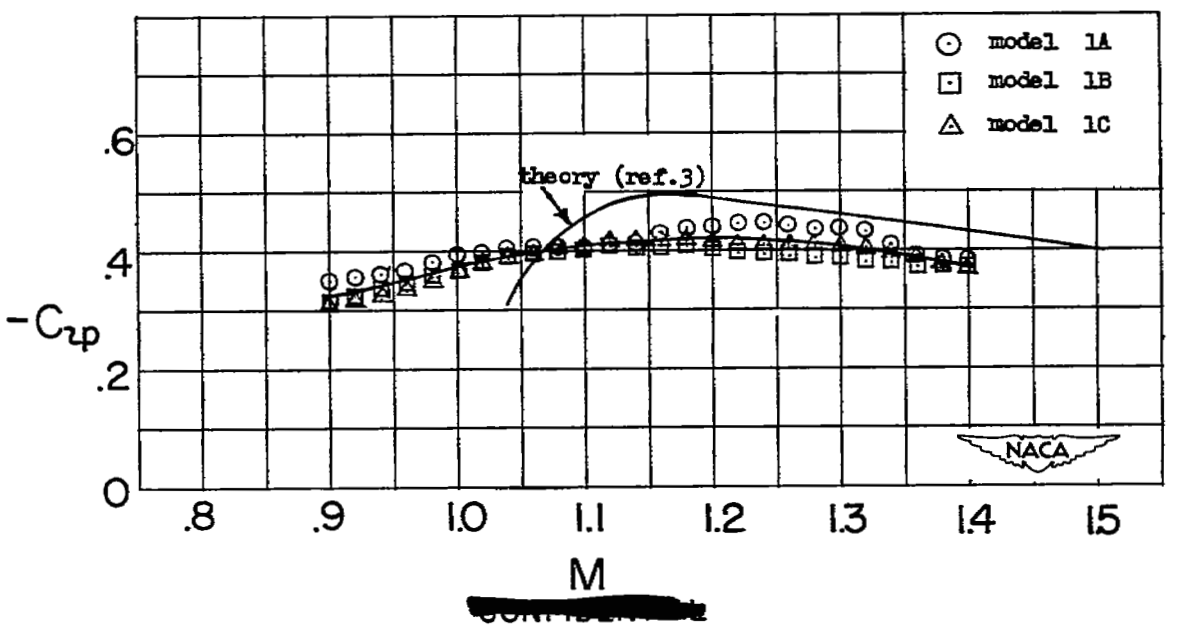

(b) NACA 65A006 airfoil section.

Figure 9.– Variation of C_{l_p} with Mach number.

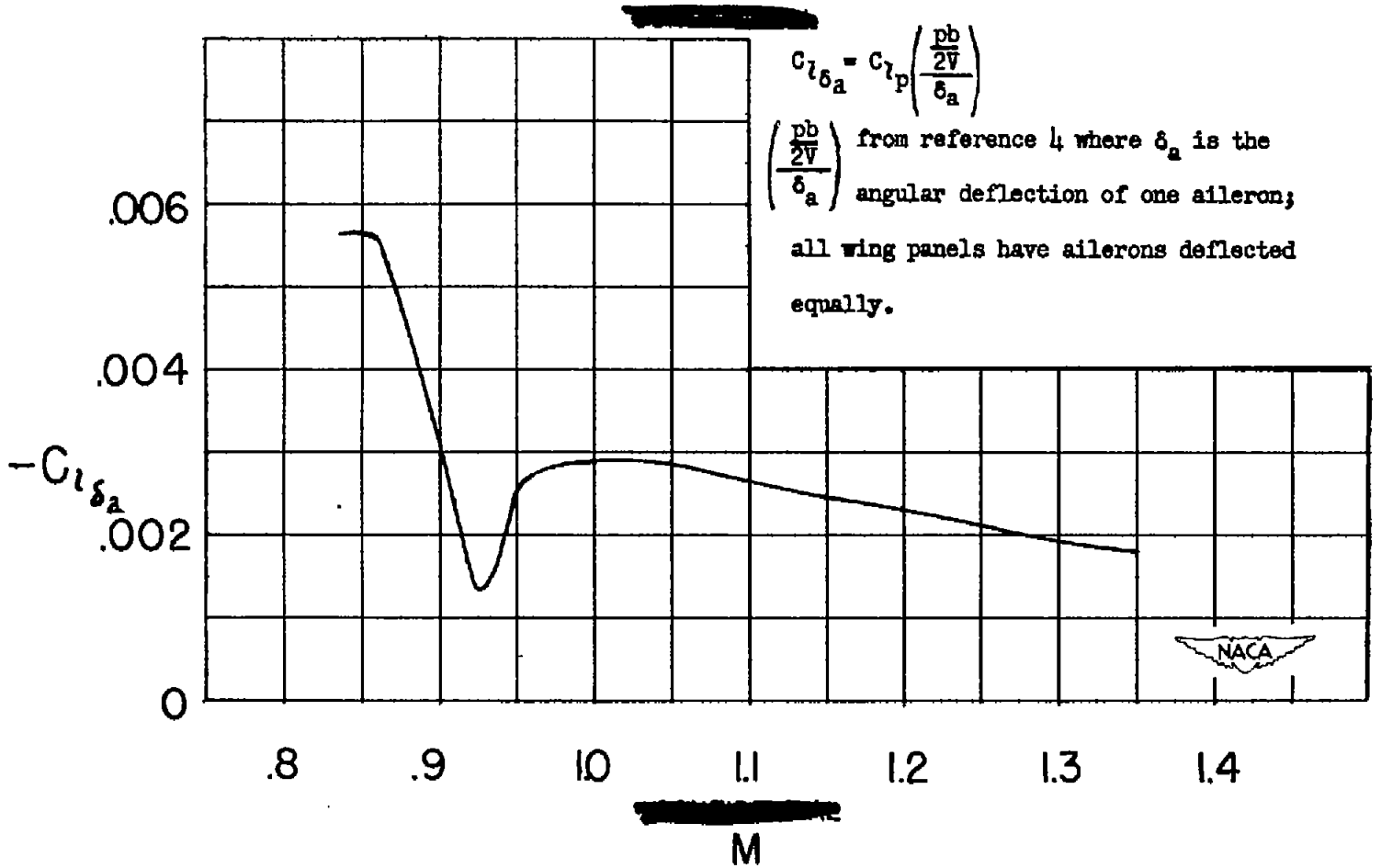

Figure 10.– Variation of rolling effectiveness with Mach number.

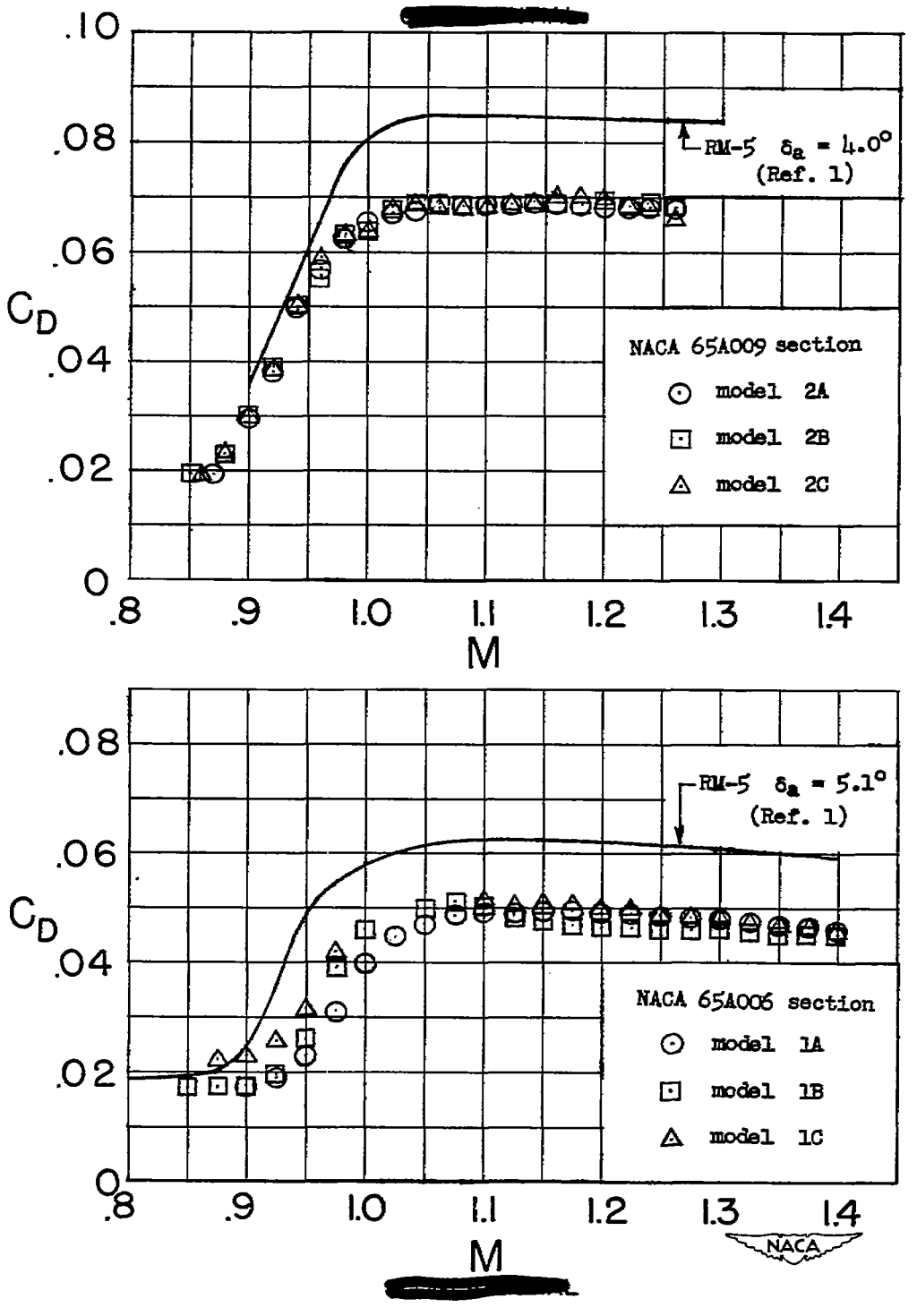

Figure 11.– Variation of total-drag coefficient with Mach number.